# Microstructure of BaRuO$_3$ thin films grown on (001) SrTiO$_3$

W. Tian and X. Q. Pan[a)]
*Department of Materials Science and Engineering, University of Michigan, Ann Arbor, Michigan 48109*

M. K. Lee and C. B. Eom
*Department of Mechanical Engineering and Materials Science, Duke University, Durham, North Carolina 27708*

BaRuO$_3$ thin films with hexagonal $4H$ structure were grown on (001) SrTiO$_3$ by a 90° off-axis rf-sputtering technique. The thin films were epitaxially grown on the (001) surface of SrTiO$_3$, with $(20\bar{2}3)$ planes parallel to the surface of the substrate. Within the growth plane, the film consists of four different crystallographic orientations with respect to the substrate, defined by the surface symmetry of the (001) SrTiO$_3$ substrate. BaRuO$_3$ grains of all four orientations show an anisotropic shape elongated along the $[\bar{1}2\bar{1}0]$ direction. The reason for the anisotropic growth is that the lattice mismatch between BaRuO$_3$ and SrTiO$_3$ is smaller along the $[\bar{1}2\bar{1}0]$ direction of SrTiO$_3$ in comparison to that along its perpendicular direction. Stacking faults and intergrowths of the $9R$ structure were observed in small local regions of the film. © *2000 American Institute of Physics.* [S0003-6951(00)03833-X]

Ternary ruthenium oxides ($A$RuO$_3$:$A$ = Ba, Sr, and Ca) have attracted increasing interest due to their unique electrical and magnetic properties, which exhibit potential applications in microelectronic devices.[1–3] The structure of $A$RuO$_3$ can be considered as a close-packed stacking of $A$O$_3$ layers in which the atomic configuration is similar to the (111) atomic plane of the cubic perovskite. The cubic close-packed stacking of $A$O$_3$ layers results in a cubic-like perovskite. In this perovskite structure, oxygen atoms form octahedra which are corner shared and filled by small Ru atoms. CaRuO$_3$ and SrRuO$_3$ belong to this structure.[4] This cubic-like structure gives rise to oxygen intermediate Ru–O–Ru bonding. In contrast, a hexagonal close-packed stacking of $A$O$_3$ layers will lead to a hexagonal structure ($2H$). In the hexagonal $2H$ structure RuO$_6$ octahedra are only face shared between different layers, giving rise to direct Ru–Ru bonding. In addition to these two extreme cases, a number of polymorphic structures can be found by mixing cubic and hexagonal stacking sequences of $A$O$_3$ layers. For instance, three different hexagonal phases were reported for BaRuO$_3$.[5,6] A four-layer hexagonal structure of BaRuO$_3$($4H$) can be formed by stacking $A$O$_3$ layers with a sequence of *CHCHCH* where ''*C*'' and ''*H*'' represent cubic and hexagonal close-packing, respectively. Similarly, the six-layer hexagonal phase of BaRuO$_3$ ($6H$) displays a stacking sequence of *CCHCCH*, and the nine-layer rhombohedral phase ($9R$) has a stacking sequence of *CHHCHHCHH*. It was found that the $9R$ phase is the most stable phase existing at atmospheric pressure with a space group of $R\bar{3}m$ (No. 166) and lattice constants $a = 5.75$ Å and $c = 21.6$ Å.[6] As pressure is increased, the $9R$ structure transforms through the $4H$ structure with a space group $P6_3/mmm$ (No. 194) and lattice constants $a = 5.73$ Å and $c = 9.5$ Å (Ref. 7) into the $6H$ structure with a space group $P6_3/mmm$ and lattice constants $a = 5.71$ Å and $c = 14.0$ Å.[8] A cubic-like perov-

skite polymorph of BaRuO$_3$ was predicted to exist as pressure is increased to approximately 120 kbar.[8]

Although the $4H$ phase is considered to be metastable, it has been successfully synthesized utilizing single-crystal-growth methods.[7,9] Recently, Lee *et al.*[10] reported the synthesis and electrical transport and magnetic properties of epitaxial thin films of *c*-axis oriented metastable $4H$ BaRuO$_3$ thin films on (111) SrTiO$_3$ substrates. It was found that the electrical properties of the $9R$ phase differ significantly from the $4H$ phase below ∼100 K. This variation of electrical properties was ascribed to the different percentage of direct Ru–Ru bonds and oxygen intermediate Ru–O–Ru bonds in the $9R$ and $4H$ phases.[9] To separate the roles of direct Ru–Ru and Ru–O–Ru bonds in determining the physical properties, it is desirable to synthesize BaRuO$_3$ with cubic-like and pure hexagonal close-packed structures.

It is well accepted that structural stabilization through thin-film epitaxy is a feasible way to form metastable phases of material.[11] Recently, Fukushima *et al.*[12] reported epitaxial growth of pseudocubic perovskite BaRuO$_3$ thin films on (001) SrTiO$_3$ substrates by means of rf sputtering. However, both x-ray diffraction[13] and the present transmission electron microscopy (TEM) studies of BaRuO$_3$ thin films, which were grown on (001) SrTiO$_3$ by 90° off-axis rf sputtering, revealed that the film has the $4H$ or/and $9R$ hexagonal structure rather than the pseudocubic perovskite structure.

In the present work, BaRuO$_3$ films were grown on (001) SrTiO$_3$ substrates using 90° off-axis sputtering. Details of the growth condition can be found elsewhere.[10] The TEM specimens were prepared by conventional cross-section TEM sample preparation procedures which ended with ion milling TEM studies were conducted with a JEOL 4000EX high-resolution transmission electron microscope (HRTEM) which has a point resolution of ∼0.17 nm.

Figure 1(a) is a low-magnification bright-field TEM image showing a cross-section view of a BaRuO$_3$ thin film grown on (001) SrTiO$_3$. The mean-film thickness was determined to be ∼320 nm. As shown in Fig. 1(a), the film has a

---
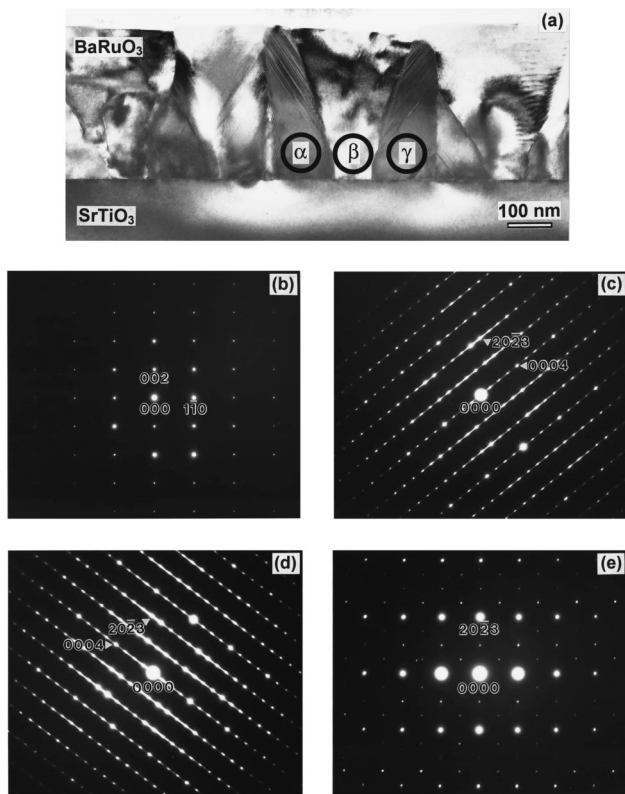
[a)]Electronic mail: panx@umich.edu

FIG. 1. (a) Bright-field cross-section TEM image of a BaRuO$_3$ film showing different columnar grains. (b) Electron-diffraction pattern along the [110] zone of the SrTiO$_3$ substrate. (c) [$\bar{1}2\bar{1}0$] zone diffraction pattern of 4H BaRuO$_3$ recorded from the grain marked by $\alpha$ in (a). (d) [$1\bar{2}10$] zone diffraction pattern taken from the grain marked by $\gamma$ in (a). (e) [$\bar{3}034$] zone diffraction pattern from the grain marked by $\beta$ in (a).

sharp interface with the substrate, but it shows a rough surface with the amplitude of height fluctuation of ~60 nm. It is also seen that the film consists of columnar grains with a mean size of ~300 nm, which is comparable with the film thickness. To identify the crystallographic orientation relationships between these BaRuO$_3$ grains and the SrTiO$_3$ substrate, selected-area electron-diffraction studies were carried out. Figure 1(b) is an electron-diffraction pattern taken from the SrTiO$_3$ substrate along the [110] zone axis. Figures 1(c), 1(d), and 1(e) are electron-diffraction patterns taken from areas marked by $\alpha$, $\gamma$, and $\beta$ in Fig. 1(a), respectively. Figures 1(c) and 1(d) are identified to be the [$\bar{1}2\bar{1}0$] and [$1\bar{2}10$] zone diffraction patterns of the hexagonal 4H structure of BaRuO$_3$, respectively. This means that grain $\alpha$ has a rotation of 180° around the film normal with respect to grain $\gamma$. Figure 1(e) was determined to be either the [$\bar{3}034$] or [$30\bar{3}\bar{4}$] zone-axis diffraction pattern of the 4H BaRuO$_3$. The weak spots in Fig. 1(e) are due to dynamic double diffractions of the crystal and from high-order Laue zones. By carefully checking the whole specimen, the electron-diffraction pattern of each grain observed in the specimen can be identified to be one of these four types of diffraction patterns. Comparing the diffraction patterns of BaRuO$_3$ films [(Figs. 1(c)–1(e)] with that of the SrTiO$_3$ substrate [Fig. 1(b)], it is concluded that all grains in the BaRuO$_3$ film are aligned with their (20$\bar{2}$3) plane parallel to the (001) surface of the substrate. This indicates that the BaRuO$_3$ thin film has the hexagonal 4H structure and grows with the (20$\bar{2}$3) plane parallel to the (001) surface of SrTiO$_3$.
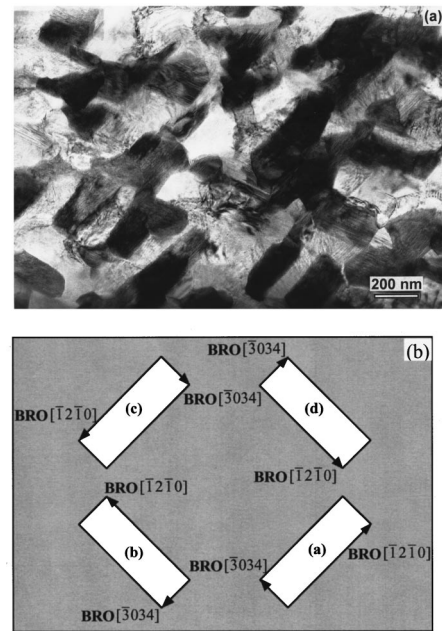


FIG. 2. (a) Plan-view TEM micrograph showing the microstructure of a BaRuO$_3$ film grown on (001) SrTiO$_3$. Note the elongated shape of the BaRuO$_3$ grains. (b) Schematic showing the BaRuO$_3$ grain arrangements on the (001) surface of SrTiO$_3$. The [$\bar{3}034$] and [$\bar{1}2\bar{1}0$] direction of BaRuO$_3$ grains are parallel to the [110] and [1$\bar{1}$0] direction of SrTiO$_3$, respectively.

BaRuO$_3$ grains with the [$\bar{3}034$] or [$30\bar{3}\bar{4}$] direction parallel the SrTiO$_3$ [110] direction cannot be distinguished in the [$\bar{3}034$] and [$30\bar{3}\bar{4}$] electron-diffraction patterns taken from a TEM specimen cut along (110) SrTiO$_3$, because these two patterns appear the same, as shown in Fig. 1(e). However, these two orientated grains can be unambiguously distinguished from each other by tilting the specimen within the TEM. Alternatively, they are distinct in the electron-diffraction pattern of a specimen cut from ($\bar{1}$10) SrTiO$_3$, in which the [$\bar{1}2\bar{1}0$] and [$1\bar{2}10$] zone-axis diffraction patterns are obtained, as shown in Figs. 1(c) and 1(d). Detailed TEM studies of both specimens showed that these four differently oriented grains in the film are randomly distributed with the same volume fraction. This was further confirmed by TEM observations of a plan-view specimen. Figure 2(a) is a plan-view TEM image of the same film as in Fig. 1. BaRuO$_3$ grains in the film are elongated along the [$\bar{1}2\bar{1}0$] direction in the plane, as shown in Fig. 2(b). This implies the existence of an anisotropic driving force for BaRuO$_3$ grain growth on (001) SrTiO$_3$.

It should be noted that the diffraction spots in Figs. 1(c) and 1(d) are strongly streaked along the $c$ direction of the 4H hexagonal structure. This results from a high density of stacking faults existing in some local regions of the BaRuO$_3$ film. The stacking faults appear as fine fringes in the cross-section TEM images, as shown in Fig. 1(a). Furthermore, high-resolution transmission electron microscopy studies reveal that the atomic stacking sequence in many (HRTEM) faulted regions, where stacking faults are periodically distributed along the $c$ axis, is in accord with that of the 9R structure. Therefore, the intergrowth of the 9R phase occurs occasionally in some small regions. Figure 3 shows a cross-section HRTEM image of a highly defective region in the film. The isolated stacking faults marked by arrows are in fact one third or two thirds of one unit cell of the 9R struc-
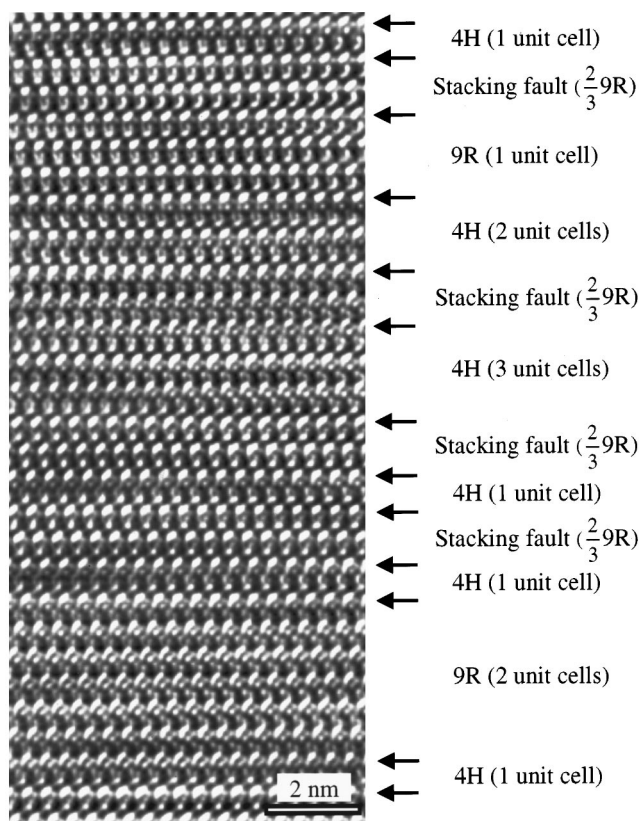
FIG. 3. HRTEM image showing the existence of stacking faults in a small region of the BaRuO$_3$ film. Segments with a thickness of 2/3, and one and two unit cells of the 9R BaRuO$_3$ *structure along the c* axis are marked.

ture along the *c* axis. As a result of the connection of these stacking faults, 9*R* phases of one or two unit cells along the *c* axis exist, as indicated by the arrows in Fig. 3. The occurrence of stacking faults and intergrowths of the 9*R* structure in the film is most likely due to the subtle difference between the formation enthalpies of 9*R* and 4*H* phases. The intergrowths are favorable because the free energy reduces with increasing the entropy in the system by the randomly layered mixture of 9*R* and 4*H* phases. However, the intergrowths of the 6*R* structure were not observed. This may suggest that the 6*R* phase has a greater formation enthalpy than the 4*H* and 9*R* phases. This is consistent with a previous study[3] which shows that the 6*R* structure is the most unstable polymorph of BaRuO$_3$.

The film microstructure and grain orientation relationships observed in TEM can be understood by considering the crystallographic structure of the BaRuO$_3$ film and the SrTiO$_3$ substrate. SrTiO$_3$ is a cubic perovskite with the space group $Pm\overline{3}m$ and lattice constant 3.905 Å. The (001) surface of SrTiO$_3$ has a fourfold rotation symmetry around the surface normal. When the 4*H*BaRuO$_3$ phase forms on the (001) surface of SrTiO$_3$ with (20$\overline{2}$3) parallel to the substrate surface, there are four different crystallographic orientations in the growth plane:

(a)   BaRuO$_3$[$\overline{3}$034]∥SrTiO$_3$[110] and
      BaRuO$_3$[$\overline{1}$2$\overline{1}$0]∥SrTiO$_3$[1$\overline{1}$0],

(b)   BaRuO$_3$[$\overline{3}$034]∥SrTiO$_3$[$\overline{1}$10] and
      BaRuO$_3$[$\overline{1}$2$\overline{1}$0]∥SrTiO$_3$[110],

(c)   BaRuO$_3$[$\overline{3}$034]∥SrTiO$_3$[$\overline{1}$$\overline{1}$0] and
      BaRuO$_3$[$\overline{1}$2$\overline{1}$0]∥SrTiO$_3$[$\overline{1}$10], and

(d)   BaRuO$_3$[$\overline{3}$034]∥SrTiO$_3$[1$\overline{1}$0] and
      BaRuO$_3$[$\overline{1}$2$\overline{1}$0]∥SrTiO$_3$[$\overline{1}$$\overline{1}$0].

These orientation relationships are in agreement with TEM observations described previously. These four orientations are crystallographically equivalent, thus, they should have an equal probability to appear in the thin film. The observed in-plane elongated grain growth may be a result of the different lattice mismatches along the two orthogonal directions between the BaRuO$_3$ film and the SrTiO$_3$ substrate. Periods of BaRuO$_3$[$\overline{1}$2$\overline{1}$0] and SrTiO$_3$ [110] are 0.573 and 0.552 nm, respectively. Moreover, the atomic arrangements along BaRuO$_3$[$\overline{1}$2$\overline{1}$0] are similar to those along SrTiO$_3$ [110]. In contrast, the period of BaRuO$_3$[$\overline{3}$034] is 4.83 nm and the atomic arrangements along this direction differ significantly from those along SrTiO$_3$ [110]. BaRuO$_3$ should prefer growing along the direction which leads to a lower interfacial misfit energy. As a consequence, the BaRuO$_3$ grains grow with an elongation along [$\overline{1}$2$\overline{1}$0].

In conclusion, it was found that the BaRuO$_3$ thin film grown on (001) SrTiO$_3$ by 90° off-axis sputtering has the hexagonal 4*H* structure. Transmission electron microscopy studies revealed that the films are grown epitaxially with the (20$\overline{2}$3) plane parallel to the (001) surface of the SrTiO$_3$ substrate. In the growth plane there exists four crystallographic equivalent orientations defined by the fourfold rotation symmetry of the (001) SrTiO$_3$ substrate surface. It was also found that BaRuO$_3$ grains show an elongation along the [$\overline{1}$2$\overline{1}$0] direction which results from the nature of structural mismatches between the BaRuO$_3$ grains and the SrTiO$_3$ substrate. Stacking faults and intergrowths of the 9*R* structure were observed in small local regions of the film.

[1] C. B. Eom, R. J. Cava, R. M. Fleming, J. M. Phillips, R. B. van Dover, J. H. Marshall, J. W. P. Hsu, J. J. Krajewski, and W. F. Peck, Jr., Science **258**, 1766 (1992).

[2] M. Shepard, S. McCall, G. Cao, and J. E. Crow, J. Appl. Phys. **81**, 4978 (1997).

[3] R. J. Bouchard and J. L. Gillson, Mater. Res. Bull. **7**, 873 (1972).

[4] H. Kobayashi, M. Nagata, R. Kanno, and Y. Kawamoto, Mater. Res. Bull. **29**, 1271 (1994).

[5] J. J. Randall and R. Ward, J. Am. Chem. Soc. **81**, 2629 (1959).

[6] P. C. Donohue, L. Katz, and R. Ward, Inorg. Chem. **4**, 306 (1965).

[7] S. T. Hong and A. W. Sleight, J. Solid State Chem. **128**, 251 (1997).

[8] J. M. Longo and J. A. Kafalas, Mater. Res. Bull. **3**, 687 (1968).

[9] J. T. Rijssenbeek, R. Jin, Y. Zadorozhny, Y. Liu, B. Batlogg, and R. J. Cava, Phys. Rev. B **59**, 4561 (1999).

[10] M. K. Lee, C. B. Eom, W. Tian, X. Q. Pan, M. Smoak, F. Tsui, and J. J. Krajewski, Appl. Phys. Lett. **77**, 364 (2000).

[11] C. P. Flynn, Phys. Rev. Lett. **57**, 599 (1986).

[12] N. Fukushima, K. Sano, T. Schimizu, K. Abe, and S. Komatsu, Appl. Phys. Lett. **73**, 1200 (1998).

[13] M. K. Lee, C. B. Eom, W. Tian, X. Q. Pan, M. C. Smoak, F. Tsui, J. Lettieri, I. W. Scrymgeour, and D. G. Schlom (unpublished).